

Characterizing two-particle entanglement in a double-well potential

Marie Bonneau,^{1,*} William J. Munro,² Kae Nemoto,³ and Jörg Schmiedmayer¹

¹*Vienna Center for Quantum Science and Technology,
Atominstitut, TU Wien, Stadionallee 2, 1020 Vienna, Austria*

²*NTT Basic Research Laboratories, 3-1 Morinosato-Wakamiya, Atsugi, Kanagawa 243-0198, Japan*

³*National Institute of Informatics, 2-1-2 Hitotsubashi, Chiyoda-ku, Tokyo 101-8430, Japan*

We consider two distinguishable atoms trapped in a double-well potential. For each atom, two orthogonal spatial modes are accessible: the states $|L\rangle$ and $|R\rangle$ spatially localized in the left and right wells respectively. We propose a method for experimentally quantifying the entanglement between these atoms and probing a violation of Bell's inequality. It is based on measuring the correlations in the atoms' momentum distribution. If the tunnelling and the energy difference between the wells are tunable, then full state tomography is achievable.

I. INTRODUCTION

A key resource necessary for the development of quantum technologies is the availability of entangled-state sources. For example in quantum optics a widely used source of entangled photons is parametric down-conversion, where twin photons are emitted in correlated spatial modes [1, 2]. In the atomic realm, twin-atom sources were developed based on atomic four-wave mixing in Bose-Einstein condensates (BEC) [3–9]. It has been demonstrated over the last years that the twin atoms are momentum-correlated [3, 4, 9] and EPR entangled [10]. Twin-atom sources have been applied to atom interferometry beyond the standard quantum limit [7, 11], to the demonstration of the Hong-Ou-Mandel effect with atoms [12] and to the generation of entanglement between different spatial regions [13–15]. The next challenge is to run these sources in configurations where single pairs of twin atoms can be used as pairs of entangled qubits. The two states of each qubit could be for example two distinct momentum modes or, if the twin atoms are generated in a double-well potential, the states $|L\rangle$ and $|R\rangle$ spatially localized in the left and right wells respectively. In this article we will consider this last configuration. Since the twin atoms are emitted in two different momentum or spin states, the two qubits are distinguishable. In parallel to twin-atom sources where multiple twin-atom pairs are emitted from a single source BEC, another approach was considered, where exactly two atoms are selected and entanglement between the spin and spatial degrees of freedom is prepared in a double-well potential [16, 17]. For twin-atom sources as well as for atom pair preparation, the resulting entangled state's quality needs to be evaluated. A method for fully characterizing the state and the entanglement of such atom pairs without making assumptions on their state is still missing.

We here present an experimentally realizable protocol for performing full tomography of two-

atom states in a double-well potential. It applies to any pure or mixed state of the Hilbert space $\mathcal{H}_{LR} = \{|L, L\rangle, |L, R\rangle, |R, L\rangle, |R, R\rangle\}$, where we note $|i, j\rangle = |i\rangle_1 \otimes |j\rangle_2$ with the indices 1 and 2 corresponding to the two atoms. Furthermore, when implementing the first part of this protocol only, one can test whether the two-atom state violates a Bell's inequality.

The situation we consider here - two atoms in a double-well potential - is an analogue to a double-slit experiment with two photons. The intensity distributions in the near-field and far-field play the role of the atom density distributions in position and momentum space. Such an experiment was first performed 30 years ago by Ghosh and Mandel [18]: They sent twin photons, entangled in momentum, through a double-slit. By measuring the two-photon coincidence detections in the far-field they observed conditional interference fringes, which were shown to be related to entanglement [19].

More recently several quantum optics experiments exploited interference patterns in coincidences for characterizing the state of two photons behind double-slits, using different approaches: In refs. [20, 21], the two photons were assumed to be in a pure state and in a specific subspace of \mathcal{H}_{LR} . Under these hypotheses, measuring the coincidences in far-field on one hand and the coincidences in near-field on the other hand allows identifying the state and quantifying directly the entanglement from the contrast of the coincidence pattern. In ref. [22], additionally, the correlations between the near- and the far-field (or in some intermediate plane) could be measured, and the two-particle density matrix was fully reconstructed for various states of \mathcal{H}_{LR} , without any assumption on these states. Finally, another method for full tomography of any state of \mathcal{H}_{LR} was demonstrated in ref. [23], where a spatial light modulator was introduced in the near-field of the slits in order to rotate the measurement basis and the coincidences were measured independently in near- and far-field.

The method of refs. [20, 21] applies to any system analogous to a double-slit where the near-field and

* mbonneau@tuwien.ac.at

far-field distributions are measured independently. An example are twin atoms in a double-well potential; another example is untrapped twin atom beams where two spatial modes are selected from each beam at the early stage of their propagation, using either Bragg selection [24] or a material mask [25], and overlap after time-of-flight (assuming the initial size of the spatial modes to be negligible with respect to their size after propagation). It was thus proposed to demonstrate the entanglement of twin atom beams emitted into given maximally entangled states from the interferences in coincidences, for example using squeezing [26] or ghost interferences [27].

We will thoroughly describe how the coincidence patterns in position and in momentum relate to the two-particle density matrix, such that for any state of \mathcal{H}_{LR} these two observable give access to most of the density matrix elements. Knowing these elements is sufficient for probing a violation of Bell's inequality in the $\{|L\rangle, |R\rangle\}$ basis. Additionally, we propose a tomography method specific to the double-well configuration. It requires to accurately manipulate the atomic external state by tuning the shape of the double-well potential [28]. Most cold atom setups with double-well trapping potentials allow tuning the tunnel coupling between the two wells from a negligible value to a regime where Josephson oscillations occur [29]. In this regime, the information encoded on the relative phase of the two wells can be transferred to their population and vice-versa. On top of this, tuning the energy difference between the two wells provides control of their relative phase. By combining these two operations before the detection of the atomic momentum distribution one can reconstruct all elements of the two-atom density matrix. With this method, performing a full tomography of two-atom states is thus remarkably simple.

Our article is organized as follow: In section II we show how the correlations of the atomic position and momentum distributions relate to the density matrix. This leads to section III where these correlations are used to set a lower bound on the system's entanglement and to section IV where they are used to probe a violation of Bell's inequality. In section V we explain how tunability of the trapping potential allows full tomography of any state of \mathcal{H}_{LR} . Finally, we describe in section VI an experimental situation for which this method could be implemented.

II. INFORMATION CONTAINED IN TWO-ATOM CORRELATIONS

Our characterization of two-atom states is inspired by the reconstruction of single-atom states in a double-well potential [28, 29]. In the later situation, the single-atom density matrix is expressed in the $\{|L\rangle, |R\rangle\}$ basis. The populations are determined from the mean in-situ

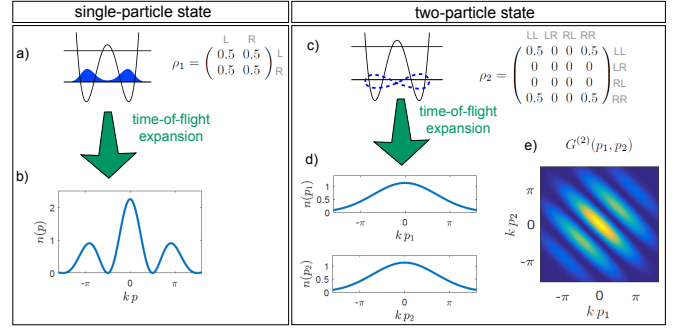


FIG. 1. Measuring the momentum distribution of atoms trapped in a double-well potential is similar to measuring the far-field intensity distribution in a double-slit experiment. For atoms in the single-particle pure state ρ_1 (left), interferences in the momentum distribution $n(p)$ (b) reflect the coherences of the density matrix and the position distribution (a) the populations. For atoms in a non-separable two-particle state (c), the mean momentum distributions $n(p_1)$, $n(p_2)$ of each particle separately (d) are not enough to characterize the state, while interferences in the momentum second-order correlation (e) relate to the coherences of the 2-particle density matrix.

density in each of the two wells, and the coherences from the mean density in momentum space. If the atoms are in a coherent superposition of the $|L\rangle$ and $|R\rangle$ states (see example in Fig. 1.a), their mean momentum distribution exhibits fringes. The fringe contrast determines the amplitude of the density matrix coherences (or at least gives a lower bound for it) and the fringe position their phase.

Considering now a two-atom state, its density matrix $\hat{\rho}$ can only be characterized when measuring two-particle properties. Since the mean density is a one-particle property, measuring it will not be sufficient for characterizing the state. For example, for a fully entangled state (see Fig. 1.b), no interference fringes are visible on the mean momentum distribution of each particle separately, since the reduced one-particle density matrix is in a totally mixed state. Therefore, in the following, we will look at the second-order correlation function

$$G^{(2)}(\xi_1, \xi_2) = \langle \hat{\Psi}^\dagger(\xi_1) \hat{\Psi}^\dagger(\xi_2) \hat{\Psi}(\xi_1) \hat{\Psi}(\xi_2) \rangle = \text{Tr}[\hat{\rho} \hat{\Psi}^\dagger(\xi_1) \hat{\Psi}^\dagger(\xi_2) \hat{\Psi}(\xi_1) \hat{\Psi}(\xi_2)] \quad (1)$$

where ξ_1 (ξ_2) is the coordinate of the first (second) atoms while the field $\hat{\Psi}(\xi_n)$ describes the n -th atom and can be expressed in the $\{|L\rangle, |R\rangle\}$ basis as

$$\hat{\Psi}(\xi_n) = \sum_{i=L,R} \Phi_i(\xi_n) \hat{a}_{ni} \quad (2)$$

with \hat{a}_{ni} being the annihilation operator of the n -th atom in the mode $|i\rangle$ of wave function Φ_i . Decomposing the two-atom density matrix as

$$\hat{\rho} = \sum_{i,j,k,l=L,R} \rho_{ijkl} |i, j\rangle \langle k, l|, \quad (3)$$

one obtains the following relation between the second-order correlation function and the elements of the density matrix:

$$G^{(2)}(\xi_1, \xi_2) = \sum_{i,j,k,l=L,R} \rho_{ijkl} \Phi_i(\xi_1) \Phi_j(\xi_2) \Phi_k^*(\xi_1) \Phi_l^*(\xi_2) \quad (4)$$

Now $G^{(2)}(\xi_1, \xi_2)$ is experimentally accessible from the density distributions $n(\xi_1)$, $n(\xi_2)$ of the first and second atom:

$$G^{(2)}(\xi_1, \xi_2) = \langle n(\xi_1) n(\xi_2) \rangle \quad (5)$$

Importantly, this requires identifying the partner of each atom, which means detecting single pairs. The coordinates ξ_1 and ξ_2 refer either to the position or to the momentum of the atoms, in both cases along the double-well axis. In analogy to the single-particle situation, the populations of $\hat{\rho}$ will be extracted from measurements of $G^{(2)}$ in position space and the coherences from interference patterns arising in $G^{(2)}$ in momentum space.

A. Correlations in position: Populations

In position space, the $|L\rangle$ and $|R\rangle$ modes are spatially separated [30]. Therefore, equation (4) simplifies to

$$G^{(2)}(x_1, x_2) = \sum_{i,j=L,R} \rho_{ijij} |\Phi_i(x_1)|^2 |\Phi_j(x_2)|^2 \quad (6)$$

When integrating over the region D_L (D_R) containing the $|L\rangle$ ($|R\rangle$) mode, one obtains the populations of the 2-atom density matrix as

$$\begin{aligned} p_{ij} &= \rho_{ijij} = \int_{D_i} dx_1 \int_{D_j} dx_2 G^{(2)}(x_1, x_2) \\ &= \int_{D_i} dx_1 \int_{D_j} dx_2 \langle n(x_1) n(x_2) \rangle \\ &= \langle n_{1i} n_{2j} \rangle \end{aligned} \quad (7)$$

where n_{1L} , n_{1R} , n_{2L} and n_{2R} are the occupations of the left and right well by the first and second atom.

B. Correlations in momentum: Coherences

Considering now the momentum space, we can rewrite equation (4) as

$$G^{(2)}(p_1, p_2) = \sum_{i,j,k,l \in \{L,R\}} \phi_{ijkl}(p_1, p_2) \rho_{ijkl} \quad (8)$$

with

$$\phi_{ijkl}(p_1, p_2) = \Phi_i(p_1) \Phi_j(p_2) \Phi_k^*(p_1) \Phi_l^*(p_2) \quad (9)$$

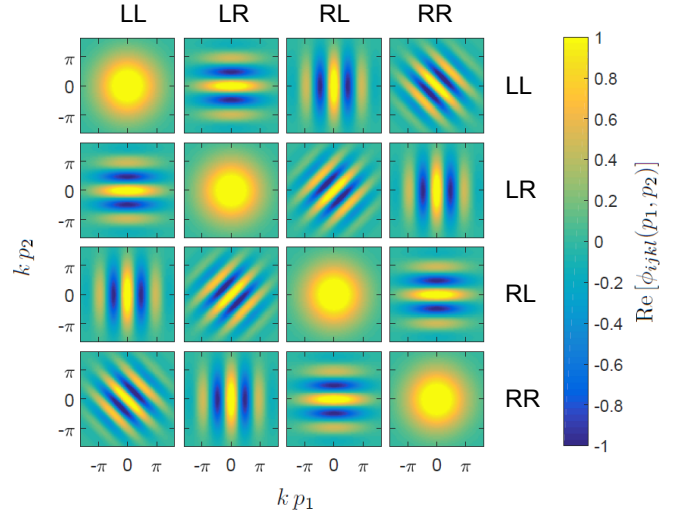


FIG. 2. The different terms ρ_{ijkl} of a two-qubit density matrix ρ contribute to the pattern of $G^{(2)}(p_1, p_2)$ with different patterns $\phi_{ijkl}(p_1, p_2)$, whose real part is plotted here.

The momentum-space wave functions of the $|L\rangle$ and $|R\rangle$ modes are $\Phi_L(p) = e^{-ikp} \times \mathcal{A}(p)$ and $\Phi_R(p) = e^{ikp} \times \mathcal{A}(p)$, where k is determined by the wells spacing. The exact shape of the envelop $\mathcal{A}(p)$ is not relevant for this discussion. For simplicity we use in Fig. 2 a Gaussian $\mathcal{A}(p) = e^{-p^2/2\sigma_p^2} \times 2/\sqrt{\pi}\sigma_p$, which is a good approximation for no tunnel coupling between the wells only. σ_p is defined by the width of the $|L\rangle$ and $|R\rangle$ wave functions in position space and is set to $0.5/k$ in Fig. 2-3.

Let us now focus on the spatial dependence of the $\phi_{ijkl}(p_1, p_2)$ functions. From Eq. (9), one gets

$$\phi_{ijkl}(p_1, p_2) = \mathcal{A}(p_1)^2 \mathcal{A}(p_2)^2 \times F_{ijkl}(p_1, p_2)$$

where $F_{ijkl}(p_1, p_2)$ is given by

$ij \backslash kl$	LL	LR	RL	RR
LL	1	e^{-2ikp_2}	e^{-2ikp_1}	$e^{-2ik(p_1+p_2)}$
LR	e^{2ikp_2}	1	$e^{-2ik(p_1-p_2)}$	e^{-2ikp_1}
RL	e^{2ikp_1}	$e^{2ik(p_1-p_2)}$	1	e^{-2ikp_2}
RR	$e^{2ik(p_1+p_2)}$	e^{2ikp_1}	e^{2ikp_2}	1

In Fig. 2 we plot the real part of the $\phi_{ijkl}(p_1, p_2)$ functions. No fringe pattern is visible for the contributions of the populations to $G^{(2)}(p_1, p_2)$, while the contributions of the coherence terms exhibit oscillations along one axis when they involve both the $|L\rangle$ and the $|R\rangle$ modes of the corresponding atom. Therefore the contributions of the anti-diagonal terms (ϕ_{LLRL} and ϕ_{LLRR}) are diagonal and antidiagonal fringes. The other coherence terms are horizontal (vertical) fringes, identical 2 by 2: $\phi_{LLRL} = \phi_{LRRR}$ and $\phi_{LRLR} = \phi_{RRRL}$. For a given state ρ , $G^{(2)}(p_1, p_2)$ is obtained by combining these contributions following Eq. (8), as shown for example on Fig. 3. Only the real part of the $\phi_{ijkl}(p_1, p_2)$ functions contribute to $G^{(2)}(p_1, p_2)$.

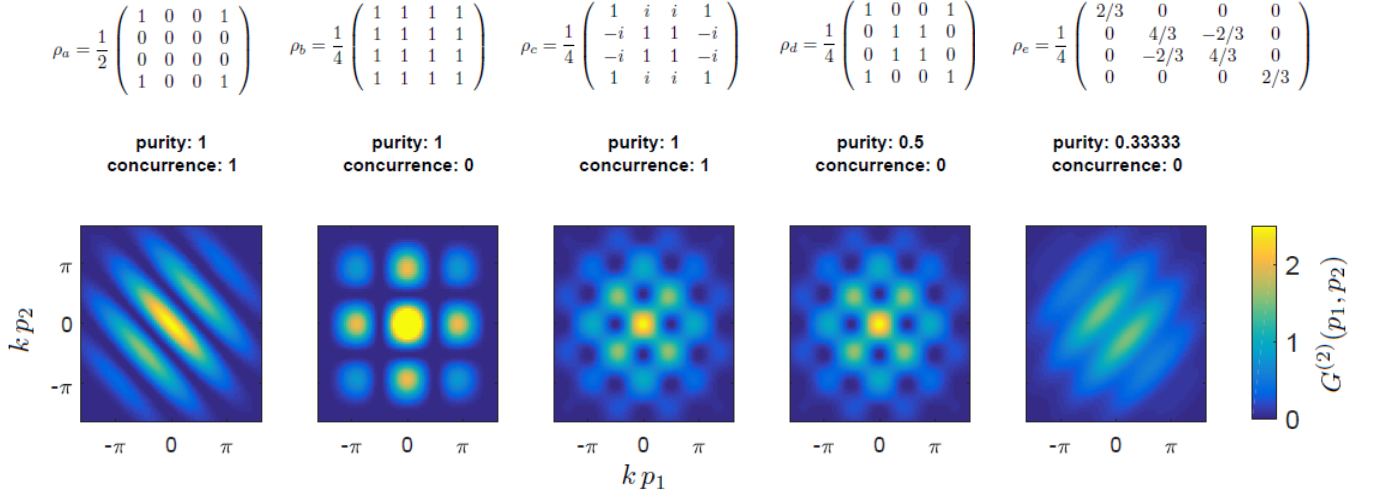


FIG. 3. Examples of correlation functions in momentum space $G^{(2)}(p_1, p_2)$ (bottom row) for two-atom states (top row) of different purities and concurrences (middle row). Spatially non-separable patterns can be obtained for entangled pure states like ρ_a and ρ_c , but also for mixed states like ρ_d and the Werner state ρ_e . For the product state ρ_b , $G^{(2)}(p_1, p_2)$ is simply the product of the oscillating mean densities of the 2 atoms. $G^{(2)}(p_1, p_2)$ provides information on some terms only of the two-atom density matrix ρ (cf text). Therefore the fully entangled state ρ_c and the fully mixed state ρ_d exhibit the same checkerboard pattern. However, in the particular case of the state ρ_a , the maximal contrast of the fringe pattern allows full reconstruction of the state.

Let us now assume that we want to characterize an unknown state of \mathcal{H}_{LR} . We have already described how the populations can be extracted from the correlations in position space. We now would like to extract information on the coherences from the correlation function in momen-

tum space. For this, we need to determine the weights of the 4 independent $\phi_{ijkl}(p_1, p_2)$ fringe patterns in the measured $G^{(2)}(p_1, p_2)$. In the following we call these weights $a = \rho_{LRRL}$, $b = \rho_{LLRR}$, $y = \rho_{LLRL} + \rho_{LRRR}$ and $z = \rho_{LLLR} + \rho_{RLRR}$. These are complex values, used as free parameters when fitting $G^{(2)}(p_1, p_2)$ by the expression

$$g(a, b, c, d, p_1, p_2) = \phi_{LLLL} + 2 \operatorname{Re}(a \times \phi_{LRRL}) + 2 \operatorname{Re}(b \times \phi_{LLRR}) + 2 \operatorname{Re}(y \times \phi_{LLRL}) + 2 \operatorname{Re}(z \times \phi_{LLLR}) \quad (10)$$

Their module is given by the amplitude of the fringes and their phase is given by the fringe position. The parameters a and b thus give us directly two of the coherence terms.

As a summary, measuring two-particle correlations in position and momentum space provides the following information on the two-atom density matrix in the $\{|L, L\rangle, |L, R\rangle, |R, L\rangle, |R, R\rangle\}$ basis (elements in bold):

$$\rho = \begin{pmatrix} \mathbf{PLL} & c & d & \mathbf{b} \\ c^* & \mathbf{PLR} & \mathbf{a} & e \\ d^* & \mathbf{a}^* & \mathbf{PRL} & f \\ \mathbf{b}^* & e^* & f^* & \mathbf{PRR} \end{pmatrix} \quad (11)$$

The complex coefficients c, d, e and f are still unknown but are linked by the constraints $c + f = z$ and $d + e = y$, where z and y are obtained from the fit. Furthermore, since ρ is a density matrix, its eigenvalues should be real and belong to $[0, 1]$. This allows setting some bounds on

the c, d, e and f coefficients. In particular, for the Bell state ρ_a of Fig. 3 (as well as for other Bell states), the above described measurements allow reconstructing the full density matrix without making any assumption on the state (the remaining coherence terms being then 0).

III. ENTANGLEMENT ESTIMATION

Although we have not yet determined the full density matrix, we can already put bounds on the entanglement of the state ρ . We quantify the entanglement with the concurrence defined as [31]:

$$C(\rho) = \max(0, \lambda_1 - \lambda_2 - \lambda_3 - \lambda_4) \quad (12)$$

with $\lambda_1 \geq \lambda_2 \geq \lambda_3 \geq \lambda_4$ the square roots of the eigenvalues of the matrix $\rho (\sigma_2^1 \otimes \sigma_2^2) \rho^* (\sigma_2^1 \otimes \sigma_2^2)$ where the matrix $\sigma_2^j = \begin{pmatrix} 0 & -i \\ i & 0 \end{pmatrix}$ applies on the j -th atom. The

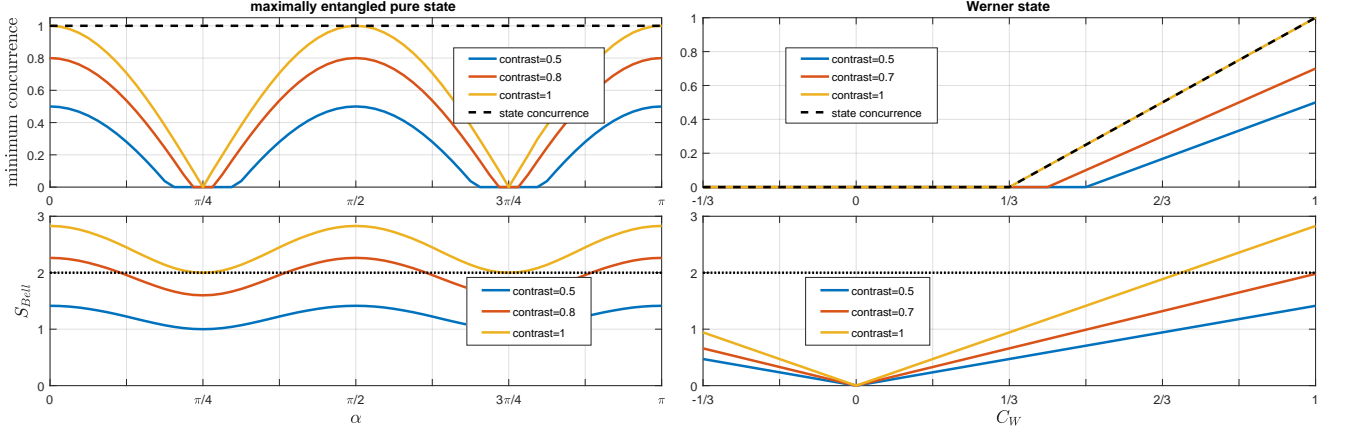


FIG. 4. left: We consider here a maximally entangled state of the form $|\Psi(\alpha)\rangle$ defined in Eq. (13). Without assuming initial knowledge on this state, the experimentally measurable correlations allow setting a lower bound on its concurrence (top), characterizing its entanglement, and computing the parameter S_{Bell} which describes a Bell inequality violation in the $\{|L\rangle, |R\rangle\}$ basis (bottom). Without experimental limitation on the fringes contrast (yellow line) one can in principle measure a maximal entanglement (the concurrence being 1) and a maximal violation of a Bell inequality ($S_{Bell} = 2\sqrt{2}$) for the Bell states $|\Psi(0)\rangle = 1/\sqrt{2}(|LL\rangle + |RR\rangle)$ and $|\Psi(\pi/2)\rangle = 1/\sqrt{2}(|LR\rangle + |RL\rangle)$. The effect of a finite experimental contrast reduces the lower bound on the concurrence and the region of the Bell violation (red and blue lines). right: In the case of a Werner state ρ_W (defined in Eq. (14)), the correlation measurement in the $\{|L\rangle, |R\rangle\}$ basis captures well the state entanglement: the lower bound on the concurrence for a perfect contrast coincides with the concurrence itself (top, yellow and dashed black lines).

concurrence is 1 for a maximally entangled state, and 0 for a non-entangled state.

Searching numerically for the values of c , d , e and f which minimize $C(\rho)$ while imposing ρ to verify the properties of a density matrix, one determines a lower bound for the concurrence. Let us consider the particular case of a maximally entangled pure state of the form

$$\begin{aligned} |\Psi(\alpha)\rangle &= \frac{1}{\sqrt{2}}(|SS\rangle + e^{2i\alpha}|AA\rangle) \\ &= \frac{1}{\sqrt{2}}\left[\cos(\alpha)(|LL\rangle + |RR\rangle) \right. \\ &\quad \left. - i\sin(\alpha)(|LR\rangle + |RL\rangle)\right] \end{aligned} \quad (13)$$

where $|S\rangle = 1/\sqrt{2}(|L\rangle + |R\rangle)$ is the (symmetric) ground state of the double-well potential and $|A\rangle = 1/\sqrt{2}(|L\rangle - |R\rangle)$ is the (antisymmetric) first excited state. As illustrated in Fig. 4 (left), the lower bound on the concurrence depends strongly on α . For $\alpha = 0$ (state ρ_a on Fig. 3) and for $\alpha = \pi/2$, one can in principle demonstrate that the state is maximally entangled. Experimentally the contrast of the atomic correlation pattern may be reduced by experimental imperfections, for example the finite resolution of the imaging system. This will reduce the lower bound for the concurrence, as illustrated on Fig. 4. On contrary, for $\alpha = \pi/4$, corresponding to the state ρ_c on Fig. 3, the correlation function is identical to the one of the fully mixed state ρ_d and therefore this method does not provide any information on the entanglement in this case. On the other side the method is perfectly suited to

characterize a Werner state defined as

$$\rho_W = \frac{1}{4} \begin{pmatrix} 1 - C_W & 0 & 0 & 0 \\ 0 & 1 + C_W & -2C_W & 0 \\ 0 & -2C_W & 1 + C_W & 0 \\ 0 & 0 & 0 & 1 - C_W \end{pmatrix} \quad (14)$$

whose degree of mixing depends on $C_W \in [-1/3, 1]$: As illustrated on Fig. 4 (right), the exact state concurrence can be determined.

IV. MEASUREMENT OF A BELL PARAMETER

Since the Bell states $|\Psi(0)\rangle = 1/\sqrt{2}(|LL\rangle + |RR\rangle)$, $|\Psi(\pi/2)\rangle = 1/\sqrt{2}(|LR\rangle + |RL\rangle)$, $1/\sqrt{2}(|LL\rangle - |RR\rangle)$ and $1/\sqrt{2}(|LR\rangle - |RL\rangle)$ can in principle be fully reconstructed from the correlation measurements, one may wonder how these measurements could allow testing a Bell's inequality. The scheme we described in this article closely relates to the scheme used by Rarity and Tapster to demonstrate a violation of a Bell's inequality in momentum for photons [32], where four momentum modes were mixed two-by-two on beam splitters and the coincidences between the outputs were measured in function of the dephasings ϕ_1 and ϕ_2 applied at one input of each beam splitter. It is formally equivalent to measure intensity at the two outputs of a beam splitter in function of an input dephasing ϕ and to measure the far-field intensity resulting from a double-slit experiment in function of the position (shifted by $\pm 1/4$ of a period, and after correction from the envelop). This is still true when measuring intensity correlations at the output of two independent

beam-splitters/double-slit systems, such that we can derive a parameter E from the values of $G^{(2)}(p_1, p_2)$ measured in 4 points:

$$E(p_1, p_2) = \frac{g_{--}^{(2)} + g_{++}^{(2)} - g_{-+}^{(2)} - g_{+-}^{(2)}}{g_{--}^{(2)} + g_{++}^{(2)} + g_{-+}^{(2)} + g_{+-}^{(2)}} \quad (15)$$

with $g_{\pm\pm}^{(2)} = G^{(2)}(p_1 \pm \pi/4k, p_2 \pm \pi/4k) / (\mathcal{A}(p_1)^2 \mathcal{A}(p_2)^2)$. From $E(p_1, p_2)$ one obtains the Bell parameter

$$S_{Bell} = \max |E(p_1, p_2) - E(p_1, p'_2) + E(p'_1, p_2) + E(p'_1, p'_2)|$$

where the maximum is taken over all $\{p_1, p'_1, p_2, p'_2\}$ configurations. The remarkable advantage of the double-slit (or double-well) configuration is that for a single experimental configuration one obtains $G^{(2)}(p_1, p_2)$ for a large range of (p_1, p_2) , while in the Rarity-Tapster scheme one needs to perform the experiment for different parameter settings (ϕ_1, ϕ_2) . Furthermore, the Bell parameter could be computed when averaging over many more points of $G^{(2)}(p_1, p_2)$, therefore reducing the associated error.

We plot on Fig. 4 (bottom left) the Bell parameter which could be computed from the correlation measurements for pure states of the form $|\Psi(\alpha)\rangle$, for different contrasts of the correlation pattern. The Bell parameter S_{Bell} is proportionnal to the contrast, such that observing a violation of a Bell's inequality ($S_{Bell} > 2$) for a Bell state (for example $|\Psi(0)\rangle$ or $|\Psi(\pi/2)\rangle$) requires a minimum contrast of $1/\sqrt{2}$. The Bell violation is thus much more sensitive on the contrast than the minimum concurrence. While being both entanglement witnesses, the Bell parameter S_{Bell} and the concurrence do not provide the same information [33]. S_{Bell} only depends on the a and b coefficients describing, for a state ρ of the form (11), the inter-well coherences shared by the two atoms: From the decomposition of Eq. (8) and due to the periodicity of the $\phi_{ijkl}(p_1, p_2)$ functions, Eq. (15) simplifies to $E(p_1, p_2) = 2 \text{Re}(a) \cos(2k(p_1 - p_2)) + 2 \text{Re}(b) \cos(2k(p_1 + p_2))$.

When measuring $G^{(2)}(p_1, p_2)$ in the far-field of the double-wells one performs thus a Bell test in the $\{|L\rangle, |R\rangle\}$ basis. While $|\Psi(\alpha)\rangle$ is always a maximally entangled state and would maximally violate a Bell inequality in the $\{|S\rangle, |A\rangle\}$ basis for any α , the Bell parameter accessible from the measurements we described depends on α and can only be maximal for the Bell states $|\Psi(0)\rangle$ and $|\Psi(\pi/2)\rangle$. These measurements are in contrast perfectly suited for the Werner state ρ_W (Fig. 4, bottom right), since its entanglement is described by the a coefficient only. The $G^{(2)}(p_1, p_2)$ measurement described in this article is thus a powerful tool to detect Bell correlations in the $\{|L\rangle, |R\rangle\}$ basis.

V. FULL TOMOGRAPHY METHOD

In order to perform a full tomography, one still needs to determine independently the c, d, e and f components of Eq. (11). We therefore would like to transform the state ρ into a state $\tilde{\rho}$ from which the initial values of c, d, e and f can be traced back. The real and imaginary parts of these parameters are accessible with two different transformations, which are easily performed in double-well potentials as depicted on Fig. 5.a-b.

For the real parts it is sufficient to perform a rotation in the $\{|L\rangle, |R\rangle\}$ basis (Fig. 5.a): When the tunnelling between the two wells is switched on, i.e. for a non-negligible energy difference Δ_{SA} between the lowest two eigenstates $|S\rangle$ and $|A\rangle$ of the double-well potential, a phase difference θ accumulates between these two states, giving rise to bosonic Josephson dynamics [29]. Each atom undergoes a rotation

$$R_i(\theta) = \begin{pmatrix} \cos \theta/2 & -i \sin \theta/2 \\ -i \sin \theta/2 & \cos \theta/2 \end{pmatrix} \quad (16)$$

such that the final density matrix is

$$\tilde{\rho}(\theta) = (R_1(\theta) \otimes R_2(\theta)) \rho (R_1(\theta)^{-1} \otimes R_2(\theta)^{-1}) \quad (17)$$

This rotated state can be characterized as described in section II and the coherences $\tilde{a}(\theta)$ and $\tilde{b}(\theta)$ extracted. We show on Fig. 5.c-d how the real parts of c, d, e and f are deduced when measuring $\tilde{a}(\pi/2)$ and $\tilde{b}(\pi/2)$.

For reconstructing the imaginary parts of c, d, e and f we introduce another transformation of the double-well potential: With an asymmetry between the left and right well (energy difference Δ_{LR} on Fig. 5.b) a phase difference ϕ between these wells accumulates linearly with time [28], transforming the state ρ into

$$\rho' = \begin{pmatrix} p_{LL} & c \times e^{i\phi} & d \times e^{i\phi} & b \times e^{2i\phi} \\ c^* \times e^{-i\phi} & p_{LR} & a & e \times e^{i\phi} \\ d^* \times e^{-i\phi} & a^* & p_{RL} & f \times e^{i\phi} \\ b^* \times e^{-2i\phi} & e^* \times e^{-i\phi} & f^* \times e^{-i\phi} & p_{RR} \end{pmatrix} \quad (18)$$

When switching the double-well potential back to the initial symmetric configuration after a delay corresponding to $\phi = \pi/2$, one gets $\text{Re}(c') = -\text{Im}(c)$ (and similarly for d, e and f) and can measure these elements when performing the rotation in the $\{|L\rangle, |R\rangle\}$ basis of Eq. (17) illustrated on Fig. 5.a.

Thus, thanks to the tunability of double-well potentials, the full density matrix can in principle be reconstructed.

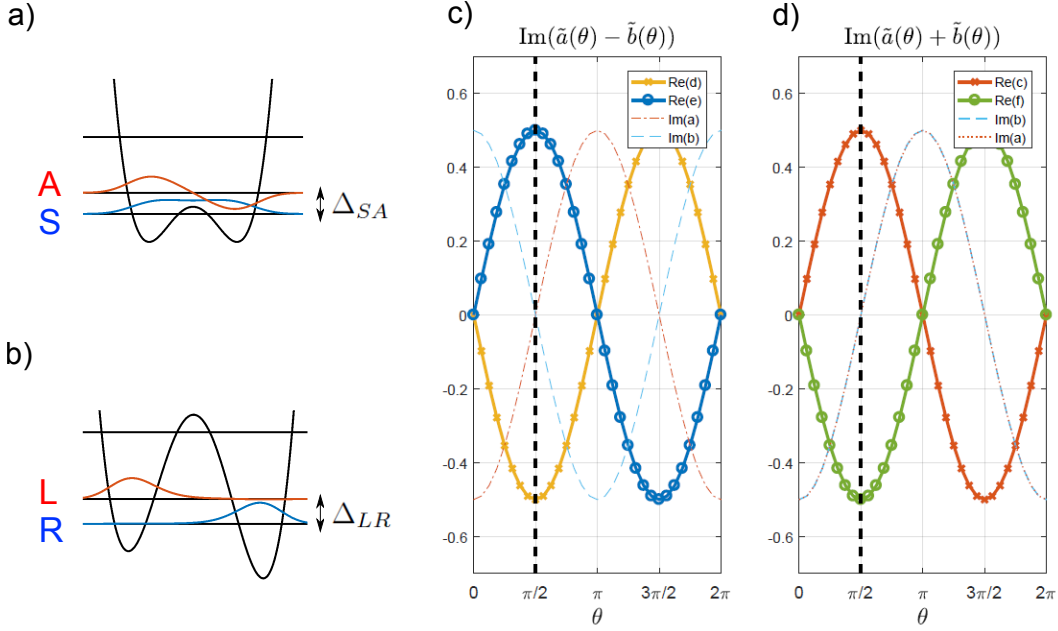


FIG. 5. By transforming the double-well potential one can perform a full tomography of the two-atom state. Two different transformations come into play: (a) In coupled double wells the atoms can tunnel and the state undergo rotation in the $\{|L\rangle, |R\rangle\}$ basis (cf Eq. (17)). (b) In decoupled, asymmetric double wells a phase difference accumulates between the left and right well. For a $\pi/2$ phase difference, the imaginary parts of the c, d, e, f elements of the initial density matrix ρ are projected onto the real part of the new density matrix ρ' (cf Eq. (18)). (c) and (d): After the rotation illustrated in (a), decomposition of the diagonal coherences of the rotated density matrix $\tilde{\rho}$ in function of the elements of the non-rotated density matrix ρ . Only the non-zero coefficients of the decomposition are plotted here. For $\theta = \pi/2$, $\text{Im}(\tilde{a} - \tilde{b}) = 1/2 \text{Re}(d - e)$ and $\text{Im}(\tilde{a} + \tilde{b}) = 1/2 \text{Re}(c - f)$. Since $d + e$ and $c + f$ are known, one can reconstruct the real parts of c, d, e and f . Applying the same operation to ρ' , one can reconstruct their imaginary parts.

VI. PROPOSED EXPERIMENTAL IMPLEMENTATION

Pairs of entangled atoms in a double-well potential can be obtained in a number of different ways. We envision here an experiment where each pair is the output of an atomic four-wave mixing process. The source is a Bose-Einstein condensate trapped in an elongated potential which has a double-well shape along one of the strongly confining axes (y), as illustrated on Fig. 6. One triggers

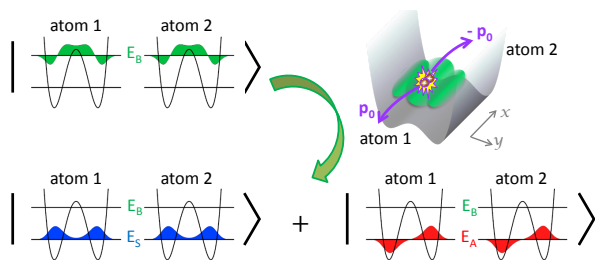


FIG. 6. An entangled two-atom state in double wells (bottom) is obtained for example through four-wave mixing, starting from a BEC in an excited transverse state of the potential (top left). The two atoms have opposite momenta $\pm p_0$ along the longitudinal axis x (top right).

the four-wave mixing process by transferring the BEC to the second excited state $|B\rangle$ of the transverse double-well potential (in green on Fig. 6). We note this state $|p_{\parallel} = 0, B\rangle$, where p_{\parallel} is the momentum along the weakly confining longitudinal axis x . This state provides two degenerate input modes for the four-wave mixing. Energy and momentum conservation select two different pairs of output modes: $|p_{\parallel} = \pm p_S, S\rangle$ where two atoms are emitted to the transverse ground state $|S\rangle$ with opposite longitudinal momenta $p_S = \sqrt{(E_B - E_S) \times 2m}$ (m being the atom mass and E_i the energy of the eigenstate $|i\rangle$ of the double-well potential) and $|p_{\parallel} = \pm p_A, A\rangle$ where two atoms are emitted to the transverse first excited state $|A\rangle$ with opposite longitudinal momenta $p_A = \sqrt{(E_B - E_A) \times 2m}$. For negligible tunnel coupling, $E_A = E_S$ such that the two pairs of output modes overlap in momentum: $p_S = p_A = p_0$. We define the first (second) atom as the one with longitudinal momentum p_0 ($-p_0$). The expected output state of the four-wave mixing is therefore the Bell state

$$\begin{aligned} |\Psi_{out}\rangle &= 1/\sqrt{2} (|SS\rangle + |AA\rangle) = |\Psi(\alpha = 0)\rangle \\ &= \frac{1}{\sqrt{2}} (|LL\rangle + |RR\rangle) \end{aligned} \quad (19)$$

From this state, any state $|\Psi(\alpha)\rangle$ (Eq. (13)) could be prepared by switching on the tunnel coupling (i.e.

the energy difference Δ_{SA} between the $|S\rangle$ and $|A\rangle$ eigenstate), as illustrated on Fig. 5.a and described in section V.

For characterizing the state we need to measure coincidences in the momentum distribution and therefore a single-atom resolution is required. Spatially-resolved single-atom detectors are based for example on fluorescence imaging combined with an EMCCD camera [34] or on multichannel-plates [35]. The spatial resolution of the imaging system is a key parameter: It could reduce the contrast of the correlation pattern fringes and prevent detecting a Bell's inequality violation. The atom momentum distribution is mapped on the position distribution at the detector after a large time of flight propagation. Our characterization method requires identifying single pairs: When working with low atom numbers source BECs and short pair production times, one reaches a regime where single-pair emission is frequent. Post-selecting such events requires a high detection efficiency, as provided by fluorescence imaging.

VII. CONCLUSION

We have described in this article various methods for characterizing 2-atom states in double-well potentials. In

contrast to what was done for photons based on analogous measurements, the only hypothesis we use here is that only the first two single-particle eigenstates of the double-well potential are accessible. We have explained how, without modifying the shape of the potential, the two-particle density matrix can be partially reconstructed from the two-particle correlations in position and momentum space and a lower bound for entanglement determined. This method is particularly interesting for strongly entangled states, since from the same measurement a Bell's inequality violation can be probed. We note that it also applies to analogous systems where each atom can occupy two modes which are separated in near-field and can interfere in far-field. We finally described how, using standard manipulations in the double-well potential, the full density matrix can be reconstructed.

VIII. ACKNOWLEDGEMENTS

MB was supported by the EU through the Marie Skłodowska Curie grant ETAB (ga no.656530) and by the FWF through the Lise Meitner grant CoPaNeq (M2088-M27). JS acknowledges support by the ERC advanced grant QuantumRelax.

-
- [1] D. Burnham and D. Weinberg, *Phys. Rev. Lett.* **25**, 84 (1970).
 - [2] S. Walborn, C. Monken, S. Pádua, and P. Souto Ribeiro, *Phys. Rep.* **495**, 87 (2010).
 - [3] A. Perrin, H. Chang, V. Krachmalnicoff, M. Schellekens, D. Boiron, A. Aspect, and C. I. Westbrook, *Phys. Rev. Lett.* **99**, 150405 (2007).
 - [4] R. Bücker, J. Grond, S. Manz, T. Berrada, T. Betz, C. Koller, U. Hohenester, T. Schumm, A. Perrin, and J. Schmiedmayer, *Nat. Phys.* **7**, 608 (2011).
 - [5] Wu RuGway, S. S. Hodgman, R. G. Dall, M. T. Johnson, and A. G. Truscott, *Phys. Rev. Lett.* **107**, 075301 (2011).
 - [6] E. M. Bookjans, C. D. Hamley, and M. S. Chapman, *Phys. Rev. Lett.* **107**, 210406 (2011).
 - [7] B. Lücke, M. Scherer, J. Kruse, L. Pezzé, F. Deuretzbacher, P. Hyllus, O. Topic, J. Peise, W. Ertmer, J. Arlt, L. Santos, A. Smerzi, and C. Klempt, *Science* **334**, 773 (2011).
 - [8] C. Gross, H. Strobel, E. Nicklas, T. Zibold, N. Bar-Gill, G. Kurizki, and M. K. Oberthaler, *Nature* **480**, 219 (2011).
 - [9] M. Bonneau, J. Ruauadel, R. Lopes, J.-C. Jaskula, A. Aspect, D. Boiron, and C. I. Westbrook, *Phys. Rev. A* **87**, 061603 (2013).
 - [10] J. Peise, I. Kruse, K. Lange, B. Lücke, L. Pezzé, J. Arlt, W. Ertmer, K. Hammerer, L. Santos, A. Smerzi, and C. Klempt, *Nat. Commun.* **6**, 8984 (2015).
 - [11] I. Kruse, K. Lange, J. Peise, B. Lücke, L. Pezzé, J. Arlt, W. Ertmer, C. Lisdat, L. Santos, A. Smerzi, and C. Klempt, *Phys. Rev. Lett.* **117**, 143004 (2016).
 - [12] R. Lopes, A. Imanaliev, A. Aspect, M. Cheneau, D. Boiron, and C. I. Westbrook, *Nature* **520**, 66 (2015).
 - [13] M. Fadel, T. Zibold, B. Décamps, and P. Treutlein, *arXiv:1708.02534* (2017).
 - [14] P. Kunkel, M. Prüfer, H. Strobel, D. Linnemann, A. Frölian, T. Gasenzer, M. Gärttner, and M. K. Oberthaler, *arXiv:1708.02407* (2017).
 - [15] K. Lange, J. Peise, B. Lücke, I. Kruse, G. Vitagliano, I. Apellaniz, M. Kleinmann, G. Toth, and C. Klempt, *arXiv:1708.02480* (2017).
 - [16] A. M. Kaufman, B. J. Lester, M. Foss-Feig, M. L. Wall, A. M. Rey, and C. A. Regal, *Nature* **527**, 208 (2015).
 - [17] S. Murmann, A. Bergschneider, V. M. Klinkhamer, G. Zürn, T. Lompe, and S. Jochim, *Phys. Rev. Lett.* **114**, 080402 (2015).
 - [18] R. Ghosh and L. Mandel, *Phys. Rev. Lett.* **59**, 1903 (1987).
 - [19] D. M. Greenberger, M. A. Horne, and A. Zeilinger, *Phys. Today* **46**, 22 (1993).
 - [20] L. Neves, G. Lima, E. J. S. Fonseca, L. Davidovich, and S. Pádua, *Phys. Rev. A* **76**, 032314 (2007).
 - [21] W. H. Peeters, J. J. Renema, and M. P. Van Exter, *Phys. Rev. A* **79**, 043817 (2009).
 - [22] G. Taguchi, T. Dougakiuchi, N. Yoshimoto, K. Kasai, M. Iinuma, H. F. Hofmann, and Y. Kadoya, *Phys. Rev. A* **78**, 012307 (2008).
 - [23] W. M. Pimenta, B. Marques, M. A. Carvalho, M. R. Barros, J. G. Fonseca, J. Ferraz, M. Terra Cunha, and S. Pádua, *Opt. Express* **18**, 24423 (2010).

- [24] P. Dussarrat, M. Perrier, A. Imanaliev, R. Lopes, A. Aspect, M. Cheneau, D. Boiron, and C. I. Westbrook, *Phys. Rev. Lett.* **119**, 173202 (2017).
- [25] R. I. Khakimov, M. Henson, K. Shin, S. S. Hodgman, R. G. Dall, K. G. H. Baldwin, and A. G. Truscott, *Nature* **540**, 100 (2016).
- [26] C. Gneiting and K. Hornberger, *Phys. Rev. Lett.* **106**, 210501 (2011).
- [27] J. Kofler, M. Singh, M. Ebner, M. Keller, M. Kotyrba, and A. Zeilinger, *Phys. Rev. A* **86**, 032115 (2012).
- [28] T. Berrada, S. van Frank, R. Bücker, T. Schumm, J.-F. Schaff, and J. Schmiedmayer, *Nat. Commun.* **4**, 2077 (2013).
- [29] M. Albiez, R. Gati, J. Fölling, S. Hunsmann, M. Cristiani, and M. K. Oberthaler, *Phys. Rev. Lett.* **95**, 010402 (2005).
- [30] Or can be mapped on spatially separated modes, as used for example in ref. [28].
- [31] W. K. Wootters, *Phys. Rev. Lett.* **80**, 2245 (1998).
- [32] J. G. Rarity and P. R. Tapster, *Phys. Rev. Lett.* **64**, 2495 (1990).
- [33] W. J. Munro, K. Nemoto, and A. G. White, *J. Mod. Opt.* **48**, 1239 (2001).
- [34] R. Bücker, A. Perrin, S. Manz, T. Betz, C. Koller, T. Plisson, J. Rottmann, T. Schumm, and J. Schmiedmayer, *New J. Phys.* **11**, 103039 (2009).
- [35] M. Schellekens, R. Hoppeler, A. Perrin, J. V. Gomes, D. Boiron, A. Aspect, and C. Westbrook, *Science* **310**, 648 (2005).